

Mitochondrial electron transport is inhibited by disappearance of metallothionein in human bronchial epithelial cells following exposure to silver nitrate

Takamitsu Miyayama^{a,*}, Yuta Arai^b, Noriyuki Suzuki^b, Seishiro Hirano^{a,b}

a, Research Center for Environmental Risk, National Institute for Environmental Studies, 16-2 Onogawa, Tsukuba, Ibaraki 305-8506, Japan

b, Graduate School of Pharmaceutical Sciences, Chiba University, 1-8-1, Inohana, Chuo, Chiba 260-8675, Japan

abstract

Silver (Ag) possesses antibacterial activity and has been used in wound dressings and deodorant powders worldwide. However, the metabolic behavior and biological roles of Ag in mammals have not been well characterized. In the present study, we exposed human bronchial epithelial cells (BEAS-2B) to AgNO₃ and investigated uptake and intracellular distribution of Ag, expression of metallothionein (MT), generation of reactive oxygen species (ROS), and changes in mitochondrial respiration. The culture medium concentration of Ag decreased with time and stabilized at 12 h. The concentration of both Ag and MT in the soluble cellular fraction increased up to 3 h and then decreased, indicating that cytosolic Ag relocated to the insoluble fraction of the cells. The levels of mRNAs for the major human MT isoforms MT-I and MT-II paralleled with the protein levels of Ag-MT. The intensity of fluorescence derived from ROS was elevated in the mitochondrial region at 24 h. Ag decreased mitochondrial oxygen consumption in a dose-dependent manner and the activity of mitochondrial complex I-IV enzymes was significantly inhibited following exposure to Ag. In a separate experiment, we found that hydrogen peroxide (H₂O₂) at concentrations as low as 0.001% (equivalent to the concentration of H₂O₂ in Ag-exposed cells) removed Ag from MT. These results suggest MT was decomposed by cytosolic H₂O₂, and then Ag released from MT relocated to insoluble cellular fractions and inhibited electron chain transfer of mitochondrial complexes, which eventually led to cell damage.

1. Introduction

Silver (Ag) has antibacterial and antifungal activities and has been used as an additive in wound dressings, catheters, bone cements, dental devices, hygiene textiles, deodorant sprays, and other consumer products. There are three main entry routes for exposure to Ag compounds: skin contact, ingestion, and inhalation. Argyria and argyrosis, chronic disorders of the skin micro-vessels and eyes in humans, arise following oral or inhalational uptake of Ag dust or colloidal silver over an extended period of time (Atiyeh et al., 2007). Studies have shown that silver metal/silver sulfide particles deposit in the skin, eyes, and other organs in workers involved in the preparation of colloidal silver-containing materials (Atiyeh et al., 2007; Lansdown, 2006). Although the cytotoxicity and intracellular distribution of Ag have been reported (Hachem et al., 2003; Hoekstra et al., 1993; Lansdown, 2006; Lansdown et al., 1997; Lansdown and Williams, 2004), very little is known about the mechanism of Ag toxicity in mammals. It has been reported that cells on the wound-healing margin actively absorb silver nitrate (AgNO_3) and that Ag binds to newly synthesized MT isoforms MT-I and MT-II, both of which are cysteine-rich proteins (Lansdown, 2002; Lansdown et al., 1997). Four major MT isoforms (MT-I, MT-II, MT-III, and MT-IV) have been identified in mammals, of which MT-I and MT-II are ubiquitously expressed (Haq et al., 2003; Kagi and Schaffer, 1988; Maret, 2000; Nordberg and Nordberg, 2000). MT isoforms are low-molecularweight (MW ~7 kDa) cytosolic proteins capable of binding a variety of essential as well as toxic metals, such as copper, zinc, cadmium, mercury, and silver. Mammalian MT isoforms contain 20 cysteine residues and 41 other amino acids; in addition, mammalian MT can bind seven zinc or cadmium ions or up to 12 copper or silver ions (Kagi and Schaffer, 1988; Maret, 2000; Nordberg and Nordberg, 2000). The basal level of MT is low in most tissues; however, synthesis of MT is markedly induced by a variety of stimuli, including metals, hormones, cytokines, oxidant-induced stress, and irradiation (Haq et al., 2003; Kagi and Schaffer, 1988; Maret, 2000; Nordberg and Nordberg, 2000). The sequence of MT isoforms is highly conserved (Haq et al., 2003), implying that MT has ubiquitous biological functions. Oxidative stress, which is characterized by an elevation in reactive oxygen species (ROS), has been implicated in a wide range of biological and pathological conditions. Cellular enzymatic processes, either in some physiological metabolic pathways (e.g., mitochondrial respiratory chain and microsomal cytochrome P450 enzymes) or disease states (e.g., xanthine oxidase in ischemiareperfusion injury) also lead to the generation of ROS (Djordjevic, 2004; Sies, 1987). Toxicity of Ag ions was reported to damage proteins thiols and generate ROS (Baldi et al., 1988). A number of cellular antioxidant systems are involved to protect cells from oxidative damage (Wilkinson et al., 2011). Recently, silver nanoparticles have gained considerable interest in application for wound bioburden reduction and in anti-inflammation, as Ag ions are released from the large surface area of nanosilver particles (White et al., 2011). Therefore, it is of importance to

investigate the mechanism of cellular responses to Ag ions for both toxicity evaluation and therapeutic application of this metal. Mitochondria are known to be a major source of ROS in cells (Bai et al., 1999). Dysfunction in electron transfer through the mitochondrial respiratory chain may result in generation of ROS species such as superoxide anion radical ($O_2^{\cdot-}$), hydrogen peroxide (H_2O_2), and the hydroxyl radical (OH^{\cdot}) (Turrens, 1997; Wang et al., 2004). Moreover, complexes I and III in the electron transport chain are thought to be responsible for ROS production because $O_2^{\cdot-}$ is formed from molecular oxygen (O_2) and then dismutated to H_2O_2 as electrons pass through the mitochondrial respiratory chain (i.e., complexes I and III) (Chen et al., 2003). In the present study, we assessed toxicity of the ionic form of Ag using human bronchial epithelial cells (BEAS-2B). We report quantitative cellular distribution of Ag, behavior of MT, and mitochondrial ROS production in Ag-exposed cells.

2. Materials and methods

2.1. Reagents

Deionized water (18.3 MΩ cm) was used in all experiments. Tris(hydroxymethyl)aminomethane (Trizma® Base) and adenosine 5'-diphosphate monopotassium salt dihydrate (ADP) were purchased from Sigma–Aldrich (St.Louis, MO, USA). Decylubiquinone was purchased from Funakoshi Co., Ltd. (Tokyo, Japan). Silver nitrate (AgNO₃), cyclohexane, HCl, potassium phosphate, NADH, MgCl₂, sucrose, sodium hydrosulfite, disodium dl-malate n-hydrate (malate), sodium hydrogen l(+)-glutamate monohydrate (glutamate), disodium succinate (succinate), 2,6-dichloroindophenol sodium salt (DCPIP), 5-methylphenazinium methyl sulfate (phenazine methosulfate), sodium dithionite, ascorbic acid, cytochrome c, and complexes I–IV inhibitors (rotenone, malonate, antimycin A, and KCN) of the highest grade were purchased from Wako Pure Chemical Industries (Osaka, Japan). A standard silver, copper, and zinc solution of atomic absorption spectrophotometry grade (1000 µg/mL; Wako Pure Chemicals Industries) was used after appropriate dilution with 0.1 mM nitric acid for calibration of concentrations of these metals.

2.2. Synthesis of decylubiquinol and reduced cytochrome c

The preparation of decylubiquinol was carried out according to Fisher's method (Fisher et al., 2004) with slight modifications. Briefly, 100 µL of 500 mM decylubiquinone was diluted in absolute ethanol to a concentration of 25 mM, after which 6 mL of a solution consisting of 0.1 M potassium phosphate buffer (pH 7.4) and 0.25 M sucrose was added. Next, 1 mL of cyclohexane and 0.1 g of solid sodium dithionite were added to the solution. The resulting solution was mixed until it turned colorless. The upper layer of cyclohexane was decanted into a separate vial. The aqueous solution was extracted twice with a 1 mL portion of cyclohexane; the organic phase was decanted after each extraction and combined with the initial organic layer. The combined organic phase was then evaporated under vacuum until a light yellowcolored syrup remained in the bottom of the tube. This syrup was dissolved in 900 µL of absolute ethanol and 100 µL of 0.1 M HCl, then stored in aliquots at –80 °C. A reduced cytochrome c stock solution was prepared by reducing cytochrome c with ascorbic acid in 10 mM potassium phosphate buffer (pH 7.0). The solution was dialyzed against 1 mL of 10 mM potassium phosphate buffer (pH 7.0) at 4 °C for 24 h using a Slide-a-Lyzer dialysis cassette (MW cutoff < 5 K; Thermo Scientific Pierce Protein Biology Products, Rockford, IL, USA) to remove the ascorbic acid. The dialysis buffer was changed every 8 h. The reduced cytochrome c stock solution was stored in a nitrogen atmosphere at –20 °C.

2.3. Cell culture

The human bronchial epithelial cell line BEAS-2B was obtained from the RIKEN Cell Bank

(Tsukuba, Japan). BEAS-2B cells were grown and maintained in DMEM Dulbecco's modified eagle's medium (DMEM) supplemented with 10% (v/v) heatinactivated fetal bovine serum (FBS, Life Technologies Japan, Ltd. Tokyo, Japan), 100 units/mL penicillin, and 100 µg/mL streptomycin at 37 °C in a 5% CO₂ atmosphere. Cells were passaged after reaching confluence using 0.05% trypsin/EDTA.

2.4. Cytotoxicity assay

Cells were seeded into a 96-well plate at 8×10^3 cells/well and were preincubated for 24 h. Cells were then exposed to AgNO₃ at a concentration of 0–100 µM for 24 h. Cytotoxicity was assessed in quadruplicate replicates using a Cell Counting Kit-8 (Dojindo Laboratories, Kumamoto, Japan) according to the manufacturer's instructions.

2.5. Measurement of Ag concentration

BEAS-2B cells were plated into 100-mm culture dishes and cultured for 24 h until reaching approximately 70% confluence. After cells were exposed to AgNO₃, the culture medium was removed and the cells were washed 3 times with PBS. Both the cells and medium were wet-digested with analytical grade nitric acid (0.75 mL) and H₂O₂ (0.25 mL) and the samples were incubated at 100 °C for 1 day in an aluminum block bath. Digested samples were diluted with deionized water and the total concentration of Ag was determined by inductively coupled plasma-mass spectrometry (ICP-MS) (7500c, Agilent Technologies, Tokyo, Japan) at m/z 107 using a standard addition method. In addition, Ag-exposed cells were collected after 24 h and suspended in 10 mM Tris-HCl, pH 7.2. To determine the distribution of Ag between the soluble and insoluble fractions of the cells, the cells were suspended and disrupted using an ultrasonic homogenizer (Bioruptor® UCD-250, CosmoBio Co., Ltd., Tokyo, Japan) for 10 min at 4 °C (H-amplitude, repeated 30-s sonications with 30-s intervals). The supernatant (soluble fraction) and the pellet (insoluble fraction) were obtained by ultracentrifugation of the homogenate at $105,000 \times g$ using a 50Ti rotor (Hitachi Koki Co., Ltd. Tokyo, Japan) for 60 min at 4 °C. These fractions were digested and the Ag concentration in each sample was determined using ICP-MS.

2.6. Chemical speciation of Ag, Cu, and Zn in the cytosolic fraction

BEAS-2B cells were plated and cultured as described above. The culture medium was replaced with fresh DMEM medium containing 1.0 µM AgNO₃. Twenty-four hours after exposure to Ag, the cells were collected using 0.05% trypsin/EDTA and suspended in 10 mM Tris-HCl, pH 7.2. The cytosolic fraction was obtained by disruption and ultracentrifugation as described above. A 20-µL aliquot of the supernatant was applied to a gel filtration column (Asahipak GS-320 HQ, 7.6 mm ID \times 300 mm; Showa Denko K.K., Tokyo, Japan), and the column was then eluted with 50 mM Tris-HCl (pH

7.2) at a flow rate of 0.5 mL/min using a Prominence HPLC system (Shimadzu Co, Kyoto, Japan). The eluate was introduced into the nebulizer of the ICP-MS. The concentrations of Ag, Cu, and Zn in the eluate were continually monitored at m/z 107, 65, and 66, respectively.

2.7. Isolation of total RNA and determination of MT-I and MT-II mRNA expression

levels using quantitative reverse transcription-polymerase chain reaction (RT-PCR) Total RNA was isolated from cells using a PureLink™ Micro-to-Midi kit (Invitrogen, Carlsbad, CA) according to the protocol provided by the manufacturer. A PrimeScript™ RT reagent kit (TaKaRa, Tokyo, Japan) was used for the reverse transcription reaction, which is the first step of real-time PCR (q-PCR). SYBR® Premix Ex Taq™ II (TaKaRa) was used for PCR. Genespecific primers used for amplification of human MT-I-A (GenBank accession no.NM 005946), MT-II-A (NM 005953), and GAPDH (NM 002046) cDNAs were as follows: MT-I-A forward (F), 5'-CTTGGGATCTCCAACCTCAC-3'; MT-I-A reverse (R), 5'-AGGTGCATTTGCACTCTTTG-3'; MT-II-A-F, 5'-ATGGATCCCAACTGCTCCT-3'; MT-II-A-R, 5'-GCATTTGCACTCTTTGCATT-3'; GAPDH-F, 5'-AATCCCATCACCATCTTCCA-3'; GAPDH-R, 5'-TGGACTCCACGACGTACTCA-3'. The following conditions were used for RT-PCR: reverse transcription reaction of cDNA at 42 °C for 15 min, denaturation with reverse transcriptase at 85 °C for 5 s followed by 40 cycles of PCR (denaturation of cDNA at 95 °C for 15 s and annealing and extension at 60 °C for 1 min). The sizes of the PCR products were 113 bp (MT-I-A), 78 bp (MT-II-A), and 82 bp (GAPDH). The amplified genes were quantified using a Thermal Cycler Dice® Real Time System TP800 (TaKaRa).

2.8. Fluorescence imaging of ROS

To assess the production of H₂O₂ and total ROS, BEAS-2B cells were seeded on 35-mm glass base dishes at a density of 2 × 10⁵ cells and pre-cultured for 24 h. The cells were further incubated with 1 μM BES-H₂O₂-Ac (Wako Pure Chemical Industries, Ltd.) for the detection of H₂O₂ or 2 μM CM-H₂DCFDA for determination of total ROS. In some experiments, cells were also loaded with 500 nM MitoTracker for 30 min to identify mitochondria. Finally, the cells were washed twice with PBS and fluorescence images were captured using confocal microscopy (TCS STED, Leica Microsystems, Wetzlar, Germany).

2.9. Isolation of rat liver mitochondria and preparation of submitochondrial particles

All animal experiments were carried out according to the Principles of Laboratory Animal Care (NIH version, revised 1996) and the Guidelines of the Animal Investigation Committee, National Institute for Environmental Studies, Japan. Threeweek-old male Sprague–Dawley rats were purchased from Clea Japan (Tokyo, Japan). The rats were maintained in an air-conditioned room

(22–25 °C and relative humidity 50–60%) with a 12-h light/dark cycle. The animals were fed a commercial diet (MF; Clea Japan) and tap water ad libitum. At 6 weeks of age, each rat (body weight = 180–200 g) was sacrificed by exsanguination under pentobarbital anesthesia and the liver was excised. The liver tissues were homogenized in nine volumes of an ice-cold buffer containing 0.23 M mannitol, 70 mM sucrose, 10 mM Tris–HCl, 1.0 mM EDTA, and 0.5% bovine serum albumin (pH 7.4) using a Teflon-pestled Potter-Elvehjem homogenizer (Thomas Scientific, Philadelphia, PA). The homogenate was first centrifuged at $700 \times g$ for 10 min and the supernatant was removed and centrifuged at $7000 \times g$ for 10 min. The pellet was washed twice and resuspended to a protein concentration of 20 mg/mL in homogenization medium without bovine serum albumin. All procedures were performed at 4 °C and the samples were stored at –80 °C until further use. The protein concentration of the sample was determined using a BCATM Protein Assay kit (Thermo Fisher Scientific, Yokohama, Japan) with bovine serum albumin as the standard. Samples were thawed on ice and submitochondrial particles (10–20 mg protein/ mL) were prepared by sonicating for three 15-s periods with 30-s intervals at an output of 40 W using an ultrasonic homogenizer (Bioruptor® UCD-250, Cosmo- Bio Co., Ltd., Tokyo, Japan) followed by centrifugation at $10,000 \times g$ for 10 min at 4 °C. The supernatant was decanted into an ultracentrifuge tube and centrifuged at $105,000 \times g$ for 30 min. The pellet (i.e., submitochondrial particles) was washed once and resuspended in buffer containing 0.23 M mannitol, 70 mM sucrose, 10 mM Tris–HCl, and 1.0 mM EDTA (pH 7.4).

2.10. Mitochondrial respiratory activity and respiratory control

Freshly isolated mitochondria were immediately used in the all mitochondrial O₂ consumption experiments without storage at –80 °C. Mitochondrial consumption of O₂ was determined polarographically with a Clark-type electrode in an air-saturated (0.24 mM O₂) reaction medium consisting of 0.23 M mannitol, 70 mM sucrose, 30 mM Tris–HCl, 4 mM MgCl₂, 5 mM Na₂HPO₄/KH₂PO₄, and 1 mM EDTA, pH 7.4 (respiration medium) and containing 1–2 mg of mitochondrial protein/mL. Uptake of O₂ was determined using 6 mM malate and glutamate as the substrate in the presence (state 3) and absence (state 4) of phosphate acceptor (0.2 mM ADP).

2.11. Assays of electron transport chain complexes (I–IV) enzyme activity

The activity of enzymes associated with complexes I–IV was determined spectrophotometrically according to published methods (Poderoso et al., 1999) using a UV-1800 spectrophotometer (Shimadzu Co.). The activity of complex I was determined in assay medium (25 mM potassium phosphate, 5 mM MgCl₂, pH 7.2) supplemented with 1 mg/mL submitochondria, 2 mM KCN, 2 µg/mL antimycin A, 40 µM decylubiquinone, and 0–10 M AgNO₃. The reaction mixture was incubated for 3 min at 4 °C, after which the temperature was raised to 30 °C and the incubation

continued for an additional 2 min. Immediately after the incubation, NADH was added to the reaction mixture to a final concentration of 130 μM . Time-course changes in oxidation of NADH was monitored at 340 nm over consecutive 16-s intervals for a period of 4 min. Treatment with 2.5 μM rotenone was used as a positive control for inhibition of complex I. The activity of enzymes associated with complex II was determined in 25 mM phosphate buffer (pH 7.8) supplemented with 20 mM succinate, 1 mM KCN, 20 μM DCPIP, 100 ng/mL submitochondria, and 0–10 μM AgNO_3 . The reaction mixture was incubated for 3 min at 4 $^\circ\text{C}$, after which the temperature was raised to 30 $^\circ\text{C}$ and the incubation continued for an additional 2 min. Immediately after the incubation, phenazine methosulfate was added to a final concentration of 450 μM . Reduction of DCPIP was monitored at 600 nm over consecutive 16-s intervals for a period of 4 min. Treatment with 1 mM malonate was used as a positive control for inhibition of complex II. The activity of enzymes associated with complex III was determined in assay medium (25 mM potassium phosphate, 5 mM MgCl_2 , pH 7.2) supplemented with 100 ng/mL submitochondria, 2 mM KCN, 2 $\mu\text{g/mL}$ rotenone, 15 μM cytochrome c, and 0–10 μM AgNO_3 . The reaction mixture was incubated for 3 min at 4 $^\circ\text{C}$, after which the temperature was raised to 30 $^\circ\text{C}$ and the incubation continued for an additional 2 min. Following the incubation, decylubiquinol was added to the reaction mixture to a final concentration of 100 μM . Reduction of cytochrome c was monitored at 550 nm over consecutive 16-s intervals for a period of 4 min. Treatment with 2 μM antimycin A was used as a positive control for inhibition of complex III. The activity of enzymes associated with complex IV was determined in 10 mM potassium phosphate (pH 7.0) supplemented with 100 ng/mL submitochondria with 0–10 μM AgNO_3 . The reaction mixture was incubated for 3 min at 4 $^\circ\text{C}$ and then the temperature was raised to 30 $^\circ\text{C}$ and the incubation continued for an additional 2 min. Reduced cytochrome c was immediately added to the reaction mixture to a final concentration of 50 μM . Oxidation of cytochrome c was monitored at 550 nm over consecutive 30 s intervals for a period of 5 min. Treatment with 2 mM KCN was used as a positive control for inhibition of complex IV.

2.12. Effect of H_2O_2 on the metal binding capacity of MT

We investigated the effect of H_2O_2 on the metal binding capacity of MT using rat hepatic MT and HPLC-ICP-MS. The liver supernatants were prepared as described above. The livers were obtained from 3-week-old Sprague–Dawley male rats and the tissues were homogenized on ice in 10 mM Tris–HCl (pH 7.4) using a glass-Teflon homogenizer. Ultracentrifugation and chemical speciation of Ag, Cu, and Zn in the supernatant were carried out as described above. A 20- μL aliquot of untreated or H_2O_2 -treated (final concentration of 0–0.0001%) supernatant was analyzed using HPLC-ICP-MS. Aliquots (20 μL) were also added to standard solutions containing 100 ppb of Ag, Cu, and Zn and the sample was introduced directly into the nebulizer tube of the HPLC-ICP-MS system. Concentrations of MT-bound Ag, Cu, and Zn were determined by integrating the signal counts for

each metal in the MT peak area using a flow injection method.

2.13. Determination of intracellular H₂O₂

The concentration of intracellular H₂O₂ was measured using a hydrogen peroxide detection kit (Fluoro H₂O₂ TM, Cell Technology Inc., Mountain View, CA) according to the manufacturer's instructions. To assess H₂O₂ levels, we observed the reagent-H₂O₂ complex (excitation = 544 nm; emission = 590 nm) using a fluorescence plate reader (POLARstar OPTIMA, BMG Labtech Ltd., Ortenberg, Germany).

2.14. Measurement of cytosolic reduced glutathione (GSH) and oxidized (GSSG)

Concentrations of cytosolic GSH and GSSG were measured using a GSH/GSSG quantification kit (Dojindo, Kumamoto, Japan) according to the manufacturer's instructions. The cells were collected by centrifugation at 200 × g for 10 min at 4 °C. The cell pellet was added with 80 μL of 10 mM HCl and they were lysed by freezing and thawing twice. The protein-free supernatant of the lysate was obtained by centrifugation (8000 × g at 4 °C). The concentration of GSSG and total glutathione was measured using 5,5'-dithiobis(2-nitrobenzoic acid) (DTNB) as a substrate in the absence and presence of GSH masking reagent, respectively. The GSH concentration was determined by subtracting the GSSG concentration from the total glutathione concentration.

2.15. Statistics

Viability values are presented as the mean ± SD of four independent cell counts. Metals concentrations were determined using triplicate wells, and each value represents the mean ± SD. Statistical analyses were performed using two-way ANOVA followed by Scheffe's post hoc examination.

3. Results

3.1. Ag concentration and distribution of Ag in BEAS-2B cells

The viability of BEAS-2B cells decreased in a dose-dependent manner following exposure to AgNO₃ (Fig. 1), with an IC₅₀ of 2.5 μM. The concentration of Ag in the culture medium decreased with time, stabilizing 12 h after Ag exposure (Fig. 2A). As shown in Table 1 and Fig. 2, about 50% of the Ag dose was taken up by the cells by 1 day after exposure. Based upon the data in Table 1 and assuming a cell diameter of 20 μm, the cellular Ag concentration was calculated to be 1.2 mM per a cell. The concentration of Ag in the soluble fraction increased up to 3 h and decreased thereafter, indicating that Ag was relocated to the insoluble fraction of the cells 3 h after exposure (Fig. 2B).

3.2. Expression of MT-I and MT-II

The distribution of Ag in the soluble fraction was determined using HPLC-ICP-MS. Fig. 3 shows elution profiles of Ag, Cu, and Zn in the cytosolic fraction of BEAS-2B cells. The peak at a retention time of 11.7 min corresponds to Cu/Zn-SOD1, while the peak at 13.2 min corresponds to Ag, Cu, and Zn bound to metallothioneins (Miyayama et al., 2008). In the elution profile of the cytosolic fraction in AgNO₃-treated BEAS-2B cells, the intensity of Ag corresponding to MT increased sharply at 3 h and then declined thereafter, whereas that of peaks representing Cu- and Zn-bound SOD1 was not altered (Fig. 3). Integration of the peak areas indicated that approximately 90% of the Ag in the cytosolic fraction was bound to MT at 3 h. The levels of mRNAs encoding the major human MT isoforms MT-I-A and MT-II-A paralleled the level of total Ag-MT protein in Ag-exposed BEAS-2B cells (Fig. 4). Although MT-I and MT-II could not be separated by the current HPLC speciation method (Fig. 4), MT-I and MT-II mRNA levels changed similarly at least in mRNA level.

3.3. Generation and localization of ROS after Ag exposure

BES-H₂O₂ was used for ROS imaging. This probe enables visualization of intracellular H₂O₂ distribution in live cells. The fluorescence intensity derived from H₂O₂ seemed to be elevated only at 24 h (Fig. 5). The cellular location (organelles) of Ag-induced ROS generation was also investigated. The ROS fluorescent probe CMH₂DCFDA and mitochondrial fluorescent probe Mito-Tracker were used simultaneously to detect ROS generation in organelles (e.g., mitochondria). Fig. 6 shows fluorescent images of ROS in BEAS-2B cells following a 24-h exposure to 1.0 μM AgNO₃. Colocalization of green fluorescence (ROS) and red fluorescence (mitochondria) as depicted by a yellow color indicates that intense ROS generation occurred in the mitochondria following treatment with Ag.

3.4. Effect of Ag exposure on mitochondrial respiration and activity of electron transport chain

complexes I–IV enzymes

The effect of Ag on respiration in rat liver submitochondrial particles was assessed by measuring O₂ consumption. Exposure to Ag resulted in a dose-dependent decrease in mitochondrial oxygen consumption (Fig. 7). To assess the effect of exposure to Ag on the activity of enzymes associated with complexes I–IV in mitochondria, submitochondrial rat liver particles were exposed to varying concentrations of Ag. The activity of enzymes associated with complexes I–IV was significantly inhibited by Ag and the specific inhibitors; 5.0 μM rotenone, 2.0 mM malonate, 4.0 μg/mL antimycin A and 4 mM KCN used as positive controls (Fig. 8). These data suggest that all four mitochondrial electron transport chain complexes are significantly affected by exposure to Ag.

3.5. Generation of H₂O₂ and stability of MT

The influence of AgNO₃ on intracellular ROS generation was assessed by determining the intracellular concentration of H₂O₂. The production of H₂O₂ increased 2.4-fold after 24 h of exposure to Ag (Fig. 9). The intracellular H₂O₂ concentration of AgNO₃-exposed cells was estimated to be 0.001% from these data, assuming that the cell diameter is 20 μm. To clarify how Ag-MT in the soluble cellular fraction is relocated to the insoluble fraction after 3 h of exposure to AgNO₃, the stability of Ag-MT in the presence of H₂O₂ was monitored using HPLC-ICP-MS. Ag ions from Ag-MT were removed by H₂O₂ treatment during the 30-min pre-incubation period. As shown in Table 2, exposure of rat liver supernatants to H₂O₂ resulted in a dose-dependent reduction in the metal binding capacity of MT. These results suggest that ROS alter the formation of Ag-binding MT and remove Ag, Cu, and Zn ions from MT-ion complexes.

3.6. Concentrations of GSH and GSSG

To determine the oxidation/reduction state in the cells, we measured the concentrations of cytosolic GSH and GSSG (Supplemental Fig. 1). GSH concentrations of AgNO₃-exposed cells were slightly increased at 24 h, whereas GSSG concentrations were not significantly change.

4. Discussion

The present study shows that AgNO₃ increases the generation of ROS in mitochondria, affects the expression of MT, and the intracellular distribution of Ag in BEAS-2B human bronchial epithelial cells. The viability of BEAS-2B cells was decreased by AgNO₃ at concentrations of 5–100 μM for 24 h (Fig. 1). Previous reports have shown that exposure to AgNO₃ at concentrations higher than 10 μM for 24 h causes a dose-dependent decrease in cell viability (Baldi et al., 1988; Hidalgo and Domínguez, 1998). The susceptibility to Ag varies among cell lines. In neuronal PC12 cells, DNA synthesis is inhibited by a 1-h exposure to 10 μM AgNO₃ (Powers et al., 2010). The viability of lymphocytes decreases significantly after exposure to 50 μM AgNO₃ (Hussain et al., 1992), while the viability of leukocytes is diminished by exposure to as low as 5 μM AgNO₃ (Jansson and Harms-Ringdahl, 1993). It has been reported that Ag interacts with a variety of biomolecules, such as nucleic acids, cell wall components, and the sulfhydryl groups of metabolic enzymes and nonenzymatic proteins such as MT and thereby inhibits proliferation and other cellular functions (Greulich et al., 2011). The Ag incorporated into cells was distributed in the cytosolic fraction and sequestered by MT 3 h after exposure to 1.0 μM AgNO₃ (Figs. 2B and 3). It has been reported that Zn and Cu ions are translocated from cytoplasm to membrane components during oxidation of MT and MT thiol groups may play a role in the protective function of MT against oxidative damage (Suntres and Lui, 2006; Thomas et al., 1986). Intracellular thiol homeostasis may play a critical role in Ag-induced lethal damage. Several studies have shown that MT plays an important role in the cellular response to heavy or transition metal-induced stress, such as that caused by exposure to Cu and Zn (Heuchel et al., 1994; Saydam et al., 2003). The affinity of the metal ions for mammalian MT follows the order of the thiolate-metal complex stability: Zn (II) < Pb (II) < Cd (II) < Cu (I), Ag (I), Hg (II) (Cortese-Krott et al., 2009; Kabzinski, 1998; Kagi and Kojima, 1987). An increase in MT is thought to lead to scavenging of Ag ions and limiting the Ag cellular distribution (Liu et al., 1991). Thus, the sensitivity of individual cells is dependent on the distribution and amount of intracellular Ag. Although we found that the level of Ag-bound MT increases sharply up to 3 h, expression of MT declined significantly thereafter (Figs. 3 and 4). Previous studies have indicated that cytoplasmic MT plays a pivotal role in protecting cells from oxidative stress induced by toxic metals and related conditions (Andrews, 2000; Klaassen et al., 2009; Liu et al., 2009; Sabolic et al., 2006). It has been reported that Zn and/or Zn-MT protect erythrocyte membranes (Min et al., 2005; Thomas et al., 1986), nucleus (Min et al., 1999), microsomes (Zhang et al., 2012), and mitochondria (Liang et al., 2012) from oxidative stress. The metal-responsive transcription factor-1 (MTF-1) is a representative transcriptional regulator for MT and it is activated under the stress of heavy metals, hypoxia and oxidation (Gunther et al., 2012). However, it has been reported that MTF-1 did not induce the MT under the excessive oxidative state in rat glial tumor (C6) cells with 20 μM Cd treatment (Nzengue et al., 2009). In this study, the time-course profile of changes in the level of Ag-bound MT was

similar to that of ROS generation (Figs. 3 and 5). Thus, it is possible to suppose that the cellular Ag-MT level was quickly decreased both by diminution of MT synthesis and by degradation of MT caused by ROS. As shown in Fig. 9 and Table 2, even 0.001% H₂O₂, which can be present in Ag-exposed cells, enhanced the release of Ag from MT. Namely, Ag is released like other metal ions (e.g., Zn and Cu) from oxidized MT. In the present study, the observed decrease in the level of MT may be due to mechanisms involving the reduction of MT synthesis and degradation of MT caused by ROS. It is contradictory that Ag is distributed to the cytoplasm in hepatoma HepG2 cells (Kim et al., 2009) and mitochondria in primary hepatocytes (Liu et al., 1991). Several cell lines of evidence also suggest that the cytotoxic effects of Ag in mitochondria are mediated via production of ROS (Foldbjerg et al., 2009; Lee et al., 2011; Miura and Shinohara, 2009; Piao et al., 2011). However, little is known about how ROS affects the distribution of Ag in mammalian cells. In the present study, ROS generation in mitochondria and the perinuclear region increased with the disappearance of Ag-MT and the increment of Ag in the insoluble fraction (Figs. 5 and 6, 2B). It has been reported that the effects of Ag on mitochondria (e.g., swelling, acceleration of mitochondrial respiration, and release of the apoptogenic protein cytochrome c) can be completely blocked by the addition of reduced thiols (e.g., GSH or dithiothreitol) (Almofti et al., 2003). Almofti et al. concluded that Ag might affect mitochondrial morphology and respiration by binding to specific thiols. MT may impede binding to Ag-specific thiols in mitochondria, as has also been discussed for other transition metal ions. Our findings are in good agreement with those of other studies describing the protective effect of MT against Ag-induced oxidative stress (Masters et al., 1994; Michalska and Choo, 1993). MT probably protects mitochondria from ROS, when MT was stably present in the cytoplasm. It has been reported that Ag interacts with GSH and subsequently the opening of the mitochondrial permeability transition pore; thereby Ag induces apoptosis (Almofti et al., 2003; Wilkinson et al., 2011). GSH was slightly increased as Ag-MT diminished (supplementary Fig. 1). It has been reported that concentrations of GSH were increased by silver treatment in mouse fibroblasts and liver cells (Arora et al., 2009). However, there is a contradictory report that the GSH level was not changed by silver in a human hepatoma cell line (Huh-7) (Cha et al., 2008). In the present study, GSH was slightly increased only at 24 h in silverexposed BEAS-2B cells. In contrast cytosolic MT concentration was remarkably decreased in response to silver exposure, suggesting that MT is more sensitive to silver-induced oxidative stress than GSH. It has been reported that dysfunction of enzymes associated with electron transport chain complexes I-IV is the main cause of ROS generation in mitochondria (Jezek and Hlavata, 2005; Liu et al., 2002; Turrens, 1997). Toxic effects of Ag are largely affected by antioxidants such as MT and GSH, because Ag⁺ is chelated by those thiol compounds. To avoid the function of these antioxidants, mitochondria from rat liver were isolated and used for Ag toxic research so that the concentration of Ag⁺ that affects mitochondrial functions would be determined. In the present study, we found that exposure to Ag resulted in a

decrease in rat liver mitochondria O₂ consumption (Fig. 7). All 4 electron transport chain complexes were inhibited in submitochondria following exposure to 0.01 μM AgNO₃ (Fig. 8), and production of H₂O₂ increased significantly following exposure to 0.1 μM AgNO₃ in BEAS-2B cells (Fig. 9). The concentration of Ag required to inhibit complexes I-IV was 10- to 100-fold lower than the lowest cytotoxic concentration (1.0 μM) shown in Fig. 1. In fact, the concentration of Ag in a single cell was calculated to be 1.2 mM based upon the data shown in Table 1 assuming that a cell diameter is 20 μm. The cellular Ag concentration was high enough to inhibit the activity of complexes I-IV enzymes under these conditions. In addition, it has been reported that mitochondria are the target organelle for other toxic elements, such as 10 μM cadmium (Wang et al., 2004) and 10–100 μM arsenical compounds (Naranmandura et al., 2011). The toxic effect of cadmium was linked to production of ROS caused by the binding of cadmium to the Qo (ubiquinol oxidizing) site of mitochondrial complex III. Arsenical compounds reportedly inhibit the activity of enzymes associated with complexes II and IV. Accordingly arsenical compounds inhibit electron transfer from complexes I and III to complexes II and IV, respectively. Ag seems to inhibit the function of mitochondrial electron transport chain complexes at lower concentrations (0.01 μM AgNO₃) than cadmium and arsenical compounds. The concentration of Ag required to inhibit complexes I-IV were orders of magnitude lower than that required for cytotoxic effects. The cell viability was not changed under the condition of 1.0 μM AgNO₃, probably because incorporated Ag was immediately sequestered by MT. On the other hand, we used isolated submitochondria in assays of electron transport chain complexes (I-IV) enzyme activity. Thus, these enzymes of submitochondria fractions may be directly influenced by AgNO₃ at a concentration as low as 0.01 μM. In summary, exposure to Ag increased MT synthesis and Ag was sequestered immediately by MT. Three hours after exposure, MT was decomposed by cytosolic H₂O₂. Ag released from MT relocated to insoluble cellular fractions and inhibited electron chain transfer of mitochondrial complexes, which eventually led to cell damage.

Conflicts of interest

There are no conflicts of interest.

Acknowledgment

This work was supported by a project grant from NIES (13230).

Appendix A. Supplementary data

Supplementary data associated with this article can be found, in the online version, at <http://dx.doi.org/10.1016/j.tox.2013.01.004>.

References

- Almofti, M.R., Ichikawa, T., Yamashita, K., Terada, H., Shinohara, Y., 2003. Silver ion induces a cyclosporine a-insensitive permeability transition in rat liver mitochondria and release of apoptogenic cytochrome c. *J. Biochem.* 134, 43–49.
- Andrews, G.K., 2000. Regulation of metallothionein gene expression by oxidative stress and metal ions. *Biochem. Pharmacol.* 59, 95–104.
- Arora, S., Jain, J., Rajwade, J.M., Paknikar, K.M., 2009. Interactions of silver nanoparticles with primary mouse fibroblasts and liver cells. *Toxicol. Appl. Pharmacol.* 236, 310–318.
- Atiyeh, B.S., Costagliola, M., Hayek, S.N., Dibo, S.A., 2007. Effect of silver on burn wound infection control and healing: review of the literature. *Burns* 33, 139–148.
- Bai, J., Rodriguez, A.M., Melendez, J.A., Cederbaum, A.I., 1999. Overexpression of catalase in cytosolic or mitochondrial compartment protects HepG2 cells against oxidative injury. *J. Biol. Chem.* 274, 26217–26224.
- Baldi, C., Minoia, C., Di Nucci, A., Capodaglio, E., Manzo, L., 1988. Effects of silver in isolated rat hepatocytes. *Toxicol. Lett.* 41, 261–268.
- Cha, K., Hong, H.W., Choi, Y.G., Lee, M.J., Park, J.H., Chae, H.K., Ryu, G., Myung, H., 2008. Comparison of acute responses of mice livers to short-term exposure to nano-sized or micro-sized silver particles. *Biotechnol. Lett.* 30, 1893–1899.
- Chen, Q., Vazquez, E.J., Moghaddas, S., Hoppel, C.L., Lesnefsky, E.J., 2003. Production of reactive oxygen species by mitochondria: central role of complex III. *J. Biol. Chem.* 278, 36027–36031.
- Cortese-Krott, M.M., Munchow, M., Pirev, E., Hessner, F., Bozkurt, A., Uciechowski, P., Pallua, N., Kroncke, K.D., Suschek, C.V., 2009. Silver ions induce oxidative stress and intracellular zinc release in human skin fibroblasts. *Free Radic. Biol. Med.* 47, 1570–1577.
- Djordjevic, V.B., 2004. Free radicals in cell biology. *Int. Rev. Cytol.* 237, 57–89.
- Fisher, N., Bourges, I., Hill, P., Brasseur, G., Meunier, B., 2004. Disruption of the interaction between the Rieske iron-sulfur protein and cytochrome b in the yeast bc1 complex owing to a human disease-associated mutation within cytochrome b. *Eur. J. Biochem.* 271, 1292–1298.
- Foldbjerg, R., Olesen, P., Hougaard, M., Dang, D.A., Hoffmann, H.J., Autrup, H., 2009. PVP-coated silver nanoparticles and silver ions induce reactive oxygen species, apoptosis and necrosis in THP-1 monocytes. *Toxicol. Lett.* 190, 156–162.
- Greulich, C., Diendorf, J., Simon, T., Eggeler, G., Epple, M., Köller, M., 2011. Uptake and intracellular distribution of silver nanoparticles in human mesenchymal stem cells. *Acta Biomater.* 7, 347–354.
- Gunther, V., Lindert, U., Schaffner, W., 2012. The taste of heavy metals: gene regulation by MTF-1. *Biochim. Biophys. Acta* 1823, 1416–1425.
- Hachem, R.Y., Wright, K.C., Zermeno, A., Bodey, G.P., Raad, I.I., 2003. Evaluation of the silver

iontophoretic catheter in an animal model. *Biomaterials* 24, 3619–3622.

Haq, F., Mahoney, M., Koropatnick, J., 2003. Signaling events for metallothionein induction. *Mutat. Res.* 533, 211–226.

Heuchel, R., Radtke, F., Georgiev, O., Stark, G., Aguet, M., Schaffner, W., 1994. The transcription factor MTF-1 is essential for basal and heavy metal-induced metallothionein gene expression. *EMBO J.* 13, 2870–2875.

Hidalgo, E., Domínguez, C., 1998. Study of cytotoxicity mechanisms of silver nitrate in human dermal fibroblasts. *Toxicol. Lett.* 98, 169–179.

Hoekstra, M.J., Hupkens, P., Dutrieux, R.P., Bosch, M.M., Brans, T.A., Kreis, R.W., 1993. A comparative burn wound model in the New Yorkshire pig for the histopathological evaluation of local therapeutic regimens: silver sulfadiazine cream as a standard. *Br. J. Plast. Surg.* 46, 585–589.

Hussain, S., Anner, R.M., Anner, B.M., 1992. Cysteine protects Na,K-ATPase and isolated human lymphocytes from silver toxicity. *Biochem. Biophys. Res. Commun.* 189, 1444–1449.

Jansson, G., Harms-Ringdahl, M., 1993. Stimulating effects of mercuric- and silver ions on the superoxide anion production in human polymorphonuclear leukocytes. *Free Radic. Res. Commun.* 18, 87–98.

Jezek, P., Hlavata, L., 2005. Mitochondria in homeostasis of reactive oxygen species in cell, tissues, and organism. *Int. J. Biochem. Cell Biol.* 37, 2478–2503.

Kabzinski, A.K., 1998. The determination of environmental and industrial exposure to heavy metals based on the quantitative isolation of metallothionein from human fluids, with application of covalent affinity chromatography with thiol-disulphide interchange gel as a solid-phase extraction support. *Talanta* 46, 335–346.

Kagi, J.H., Kojima, Y., 1987. Chemistry and biochemistry of metallothionein. *Exp. Suppl.* 52, 25–61.

Kagi, J.H., Schaffer, A., 1988. Biochemistry of metallothionein. *Biochemistry* 27, 8509–8515.

Kim, S., Choi, J.E., Choi, J., Chung, K.H., Park, K., Yi, J., Ryu, D.Y., 2009. Oxidative stress-dependent toxicity of silver nanoparticles in human hepatoma cells. *Toxicol. In Vitro* 23, 1076–1084.

Klaassen, C.D., Liu, J., Diwan, B.A., 2009. Metallothionein protection of cadmium toxicity. *Toxicol. Appl. Pharmacol.* 238, 215–220.

Lansdown, A.B., 2002. Metallothioneins: potential therapeutic aids for wound healing in the skin. *Wound Rep. Regen.* 10, 130–132.

Lansdown, A.B., 2006. Silver in health care: antimicrobial effects and safety in use. *Curr. Probl. Dermatol.* 33, 17–34.

Lansdown, A.B., Williams, A., 2004. How safe is silver in wound care. *J. Wound Care* 13, 131–136.

Lansdown, A.B., Sampson, B., Laupattarakasem, P., Vuttivirojana, A., 1997. Silver aids healing in

the sterile skin wound: experimental studies in the laboratory rat. *Br. J. Dermatol.* 137, 728–735.

Lee, Y.S., Kim, D.W., Lee, Y.H., Oh, J.H., Yoon, S., Choi, M.S., Lee, S.K., Kim, J.W., Lee, K., Song, C.W., 2011. Silver nanoparticles induce apoptosis and G2/M arrest via PKCzeta-dependent signaling in A549 lung cells. *Arch. Toxicol.* 85, 1529–1540.

Liang, D., Yang, M., Guo, B., Cao, J., Yang, L., Guo, X., Li, Y., Gao, Z., 2012. Zinc inhibits H₂O₂-induced MC3T3-E1 cells apoptosis via MAPK and PI3K/AKT pathways. *Biol. Trace Elem. Res.* 148, 420–429.

Liu, J., Kershaw, W.C., Klaassen, C.D., 1991. The protective effect of metallothionein on the toxicity of various metals in rat primary hepatocyte culture. *Toxicol. Appl. Pharmacol.* 107, 27–34.

Liu, Y., Fiskum, G., Schubert, D., 2002. Generation of reactive oxygen species by the mitochondrial electron transport chain. *J. Neurochem.* 80, 780–787.

Liu, J., Qu, W., Kadiiska, M.B., 2009. Role of oxidative stress in cadmium toxicity and carcinogenesis. *Toxicol. Appl. Pharmacol.* 238, 209–214.

Maret, W., 2000. The function of zinc metallothionein: a link between cellular zinc and redox state. *J. Nutr.* 130, 1455S–1458S.

Masters, B.A., Kelly, E.J., Quaife, C.J., Brinster, R.L., Palmiter, R.D., 1994. Targeted disruption of metallothionein I and II genes increases sensitivity to cadmium. *Proc. Natl. Acad. Sci. U.S.A.* 91, 584–588.

Michalska, A.E., Choo, K.H., 1993. Targeting and germ-line transmission of a null mutation at the metallothionein I and II loci in mouse. *Proc. Natl. Acad. Sci. U.S.A.* 90, 8088–8092.

Min, K.S., Nishida, K., Onosaka, S., 1999. Protective effect of metallothionein to ras DNA damage induced by hydrogen peroxide and ferric ion-nitrilotriacetic acid. *Chem. Biol. Interact.* 122, 137–152.

Min, K.S., Tanaka, N., Horie, T., Kawano, H., Tetsuchikawahara, N., Onosaka, S., 2005. Metallothionein-enriched hepatocytes are resistant to ferric nitriloacetate toxicity during conditions of glutathione depletion. *Toxicol. Lett.* 158, 108–115.

Miura, N., Shinohara, Y., 2009. Cytotoxic effect and apoptosis induction by silver nanoparticles in HeLa cells. *Biochem. Biophys. Res. Commun.* 390, 733–737.

Miyayama, T., Ogra, Y., Osima, Y., Suzuki, K.T., 2008. Narrow-bore HPLC-ICP-MS for speciation of copper in mutant mouse neonates bearing a defect in Cu metabolism. *Anal. Bioanal. Chem.* 390, 1799–1803.

Naranmandura, H., Xu, S., Sawata, T., Hao, W.H., Liu, H., Bu, N., Ogra, Y., Lou, Y.J., Suzuki, N., 2011. Mitochondria are the main target organelle for trivalent monomethylarsonous acid (MMA(III))-induced cytotoxicity. *Chem. Res. Toxicol.* 24, 1094–1103.

Nordberg, M., Nordberg, G.F., 2000. Toxicological aspects of metallothionein. *Cell. Mol. Biol. (Noisy-le-grand)* 46, 451–463.

Nzengue, Y., Lefebvre, E., Cadet, J., Favier, A., Rachidi, W., Steiman, R., Guiraud, P., 2009. Metallothionein expression in HaCaT and C6 cell lines exposed to cadmium. *J. Trace Elem. Med. Biol.* 23, 314–323.

Piao, M.J., Kang, K.A., Lee, I.K., Kim, H.S., Kim, S., Choi, J.Y., Choi, J., Hyun, J.W., 2011. Silver nanoparticles induce oxidative cell damage in human liver cells through inhibition of reduced glutathione and induction of mitochondria-involved apoptosis. *Toxicol. Lett.* 201, 92–100.

Poderoso, J.J., Lisdero, C., Schopfer, F., Riobo, N., Carreras, M.C., Cadenas, E., Boveris, A., 1999. The regulation of mitochondrial oxygen uptake by redox reactions involving nitric oxide and ubiquinol. *J. Biol. Chem.* 274, 37709–37716.

Powers, C.M., Wrench, N., Ryde, I.T., Smith, A.M., Seidler, F.J., Slotkin, T.A., 2010. Silver impairs neurodevelopment: studies in PC12 cells. *Environ. Health Perspect.* 118, 73–79.

Sabolic, I., Herak-Kramberger, C.M., Antolovic, R., Breton, S., Brown, D., 2006. Loss of basolateral invaginations in proximal tubules of cadmium-intoxicated rats is independent of microtubules and clathrin. *Toxicology* 218, 149–163.

Saydam, N., Steiner, F., Georgiev, O., Schaffner, W., 2003. Heat and heavy metal stress synergize to mediate transcriptional hyperactivation by metal-responsive transcription factor MTF-1. *J. Biol. Chem.* 278, 31879–31883.

Sies, H., 1987. Antioxidant activity in cells and organs. *Am. Rev. Respir. Dis.* 136, 478–480.

Suntres, Z.E., Lui, E.M., 2006. Prooxidative effect of copper – metallothionein in the acute cytotoxicity of hydrogen peroxide in Ehrlich ascites tumour cells. *Toxicology* 217, 155–168.

Thomas, J.P., Bachowski, G.J., Girotti, A.W., 1986. Inhibition of cell membrane lipid peroxidation by cadmium- and zinc-metallothioneins. *Biochim. Biophys. Acta* 884, 448–461.

Turrens, J.F., 1997. Superoxide production by the mitochondrial respiratory chain. *Biosci. Rep.* 17, 3–8.

Wang, Y., Fang, J., Leonard, S.S., Rao, K.M., 2004. Cadmium inhibits the electron transfer chain and induces reactive oxygen species. *Free Radic. Biol. Med.* 36, 1434–1443.

White, R.J., Fumarola, S., Denyer, J., 2011. Interim advice on silver dressings in neonatal/paediatric wound and skin care. *J. Wound Care* 20, 192.

Wilkinson, L.J., White, R.J., Chipman, J.K., 2011. Silver and nanoparticles of silver in wound dressings: a review of efficacy and safety. *J. Wound Care* 20, 543–549.

Zhang, Y., Hu, N., Hua, Y., Richmond, K.L., Dong, F., Ren, J., 2012. Cardiac overexpression of metallothionein rescues cold exposure-induced myocardial contractile dysfunction through attenuation of cardiac fibrosis despite cardiomyocyte mechanical anomalies. *Free Radic. Biol. Med.* 53, 194–207.

Tables

Table 1 Concentration of Ag in BEAS-2B cells after exposure to 0 μM or 1.0 μM AgNO_3 for 24 h. The concentration of Ag was determined using ICP-MS (m/z 107). Data are expressed as the mean \pm SD (n = 3).

Table 2 Changes in the Ag, Cu, and Zn content in MT following exposure to H_2O_2 . The amount (pmol) of Ag, Cu, and Zn in MT peak areas after treatment with H_2O_2 was determined using flow injection by HPLC-ICP-MS (m/z 107, 65, and 66, respectively, for Ag, Cu, and Zn). Data are expressed as the mean \pm SD (n = 3).

Table 1

Ag concentration ($\mu\text{g Ag/mg protein}$)	
Control	0.00583 ± 0.00158
AgNO ₃	11.4 ± 0.885
Ag concentration ($\text{ng Ag}/1.0 \times 10^5 \text{ cells}$)	
Control	0.0219 ± 0.00693
AgNO ₃	56.1 ± 0.170

Table 2

H ₂ O ₂ (%)	Ag (pmol)	Cu (pmol)	Zn (pmol)
0	225.66 ± 10.53	20.22 ± 0.46	133.18 ± 8.19
0.0001	81.16 ± 3.69	14.41 ± 0.70	71.27 ± 7.72
0.001	69.50 ± 5.64	10.66 ± 0.47	62.30 ± 9.90
0.01	63.42 ± 4.04	7.43 ± 0.73	57.59 ± 2.43
0.1	54.23 ± 3.40	5.37 ± 0.21	31.12 ± 1.29

Figures

Fig. 1. Cytotoxic effect of AgNO₃. BEAS-2B cells were treated with 0, 0.05, 0.1, 0.5, 1.0, 5.0, 10, 50, or 100 μ M AgNO₃ for 24 h. Data are expressed as the mean \pm SD (n = 4). (*) Significantly different from control group (P < 0.05).

Fig. 2. Changes in Ag concentration of the culture medium following treatment of BEAS-2B cells with 1.0 μ M AgNO₃ for 0, 3, 6, 12, and 24 h (A) and subcellular distribution of Ag in BEAS-2B cells treated with AgNO₃ (B). Concentrations of Ag in the medium or soluble and insoluble fractions of the cells were determined using ICP-MS (m/z 107). Data are expressed as the mean \pm SD (n = 3). In (A), (*) denotes significantly different from 0-h group (P < 0.05); (#) denotes significantly different from 3-h group (P < 0.05); and (§) denotes significantly different from 6-h group (P < 0.05). In (B), (*) denotes significantly different from 3-h group in soluble fraction (P < 0.05); (#) denotes significantly different from 6-h group in soluble fraction (P < 0.05); (§) denotes significantly different from 3-h group in insoluble fraction (P < 0.05); (†) denotes significantly different from 6-h group in insoluble fraction (P < 0.05); and (‡) denotes significantly different from 12-h group in insoluble fraction (P < 0.05).

Fig. 3. Elution profiles of Ag, Cu, and Zn in the cytosolic fraction of BEAS-2B cells treated with 1.0 μ M AgNO₃, as determined by HPLC-ICP-MS. Cells were treated with AgNO₃ (1.0 μ M) for 0, 3, 6, 12, and 24 h. The HPLC system was equipped with a multi-mode gel filtration column (Shodex GS320HQ). A 20- μ L aliquot of the cytosolic fraction was applied to the column and the column was eluted with 50 mM Tris-HCl, pH 7.2, at a flow rate of 0.5 mL/min. The concentrations of Ag, Cu, and Zn in the eluate were continually monitored at m/z 107 (1 count = 4.79×10^{-2} fmol), 65 (1 count = 4.34×10^{-2} fmol), and 66 (1 count = 2.58×10^{-2} fmol), respectively.

Fig. 4. Effect of AgNO₃ on MT-I-A and MT-II-A mRNA expression in BEAS-2B cells. BEAS-2B cells were treated with 1.0 μ M AgNO₃ for 0, 3, 6, 12, and 24 h, after which total RNA was isolated from the cells. The expression of MT-I-A and MT-II-A mRNA was quantified using real time PCR and the data were normalized against the level of GAPDH mRNA. Data are expressed as the mean \pm SD (n = 3). P < 0.05 was considered significant. In MT-I-A, (*) denotes significantly different from 0-h group (P < 0.05); (#) denotes significantly different from 3-h group (P < 0.05); (§) denotes significantly different from 6-h group (P < 0.05). In MT-II-A, (*) denotes significantly different from 0-h group (P < 0.05); (#) denotes significantly different from 3-h group (P < 0.05); (§) denotes significantly different from 6-h group (P < 0.05).

Fig. 5. Fluorescence imaging of H₂O₂ in BEAS-2B cells treated with AgNO₃. BEAS-2B cells were incubated with 1.0 μM AgNO₃ for 0, 3, and 24 h. The cells were loaded with BES-H₂O₂ and fluorescence derived from H₂O₂-BES-H₂O₂ complexes was detected by fluorescence microscopy and digital images were captured using a cellSens® Standard system.

Fig. 6. Localization of reactive oxygen species (ROS) in BEAS-2B cells after exposure to AgNO₃. Cells were incubated with 1.0 μM AgNO₃ for 0, 3, and 24 h and then exposed to 2 μM CM-H₂DCFDA and 500 nM Mito Tracker for 30 min. Localization of ROS was determined by superimposing green fluorescence (DCFDA-derived CM-H₂DCFDA) and red fluorescence (Mito Tracker).

Fig. 7. Effect of Ag on rat liver mitochondrial respiration. Rat liver mitochondria (1 mg protein/mL) were incubated at 30 °C in reaction medium containing 6 mM malate/glutamate with (B) or without (C) 0.1 mM ADP. The complete sample was pre-incubated for 5 min with 10, 1.0, 0.1 and 0.01 μM AgNO₃, respectively (D–G). Sodium hydrosulfite is a potent reducing agent capable of removing oxygen from reaction medium lacking mitochondria (A)

Fig. 8. Effect of Ag on the activity of enzymes associated with electron transport chain complexes I–IV. The activity of complexes I–IV enzymes was assessed according to the procedure described in Section 2. NADH reduction (complex I), DCPIP reduction (complex II), reduction (complex III) and oxidation (complex IV) of Cytochrome c were monitored by UV spectrophotometer at 340, 600, and 550 nm, respectively. The specific inhibitors were exposed to 2.5 μM rotenone, 1 mM malonate, 2 μg/mL antimycin A, and 2 mM KCN. Data are expressed as the mean ± SD (n = 3) of percentage of the control value. Statistical significance was assessed using two-way ANOVA and followed by Scheffe's post hoc test; P < 0.05 was considered significant. (*) Significantly different from control group (P < 0.05). (#) Significantly different from individual inhibitors group (P < 0.05). (§) Significantly different from 10 μM AgNO₃ group (P < 0.05). (†) Significantly different from 1.0 μM AgNO₃ group (P < 0.05). (‡) Significantly different from 0.1 μM AgNO₃ group (P < 0.05).

Fig. 9. Intracellular ROS generation in Ag-exposed BEAS-2B cells. Cells were exposed to 0–1.0 μM AgNO₃ for 24 h and H₂O₂-derived fluorescence was measured. Each bar represents the mean ± SD (n = 6). Statistical significance was determined using two-way ANOVA and followed by Scheffe's post hoc test; P < 0.05 was considered significant. (*) Significantly different from 1.0 μM AgNO₃ group (P < 0.05).

Fig.1

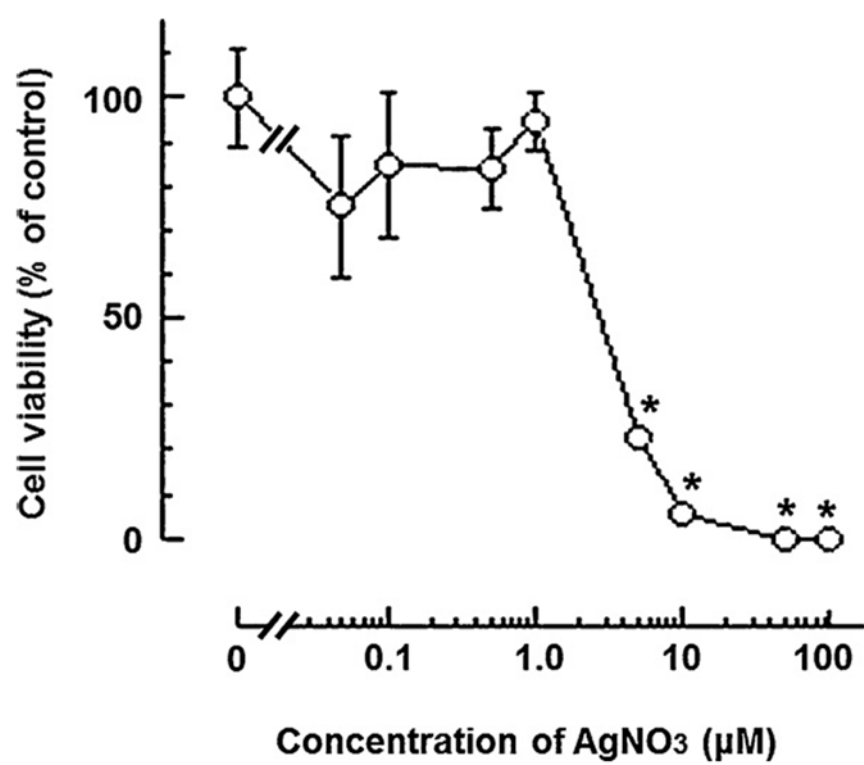


Fig.2

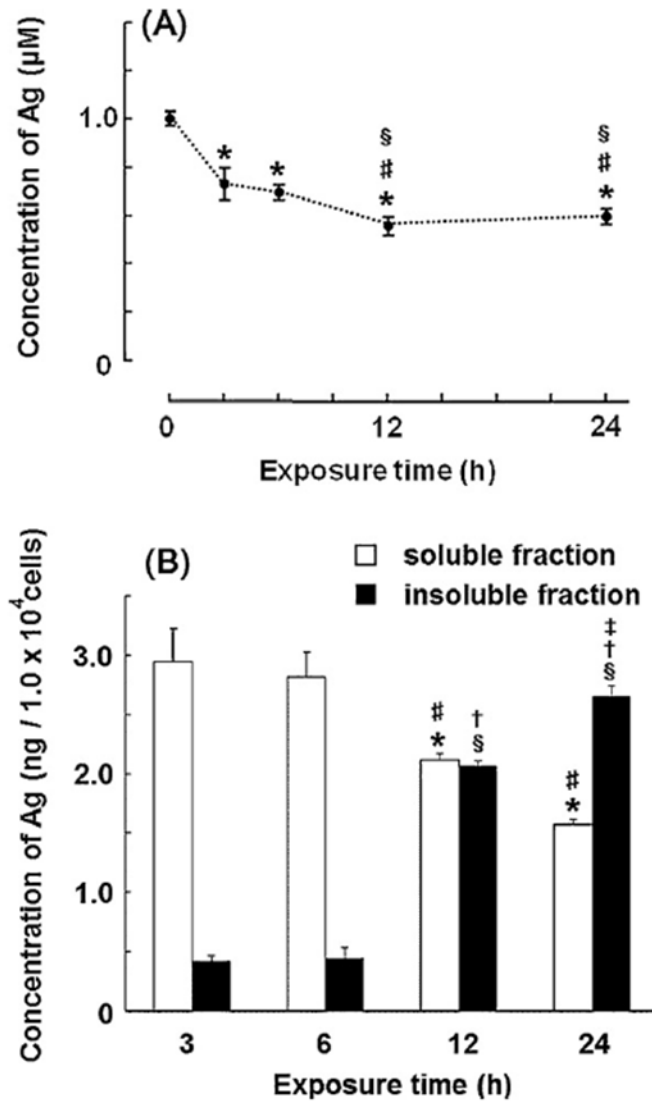


Fig.3

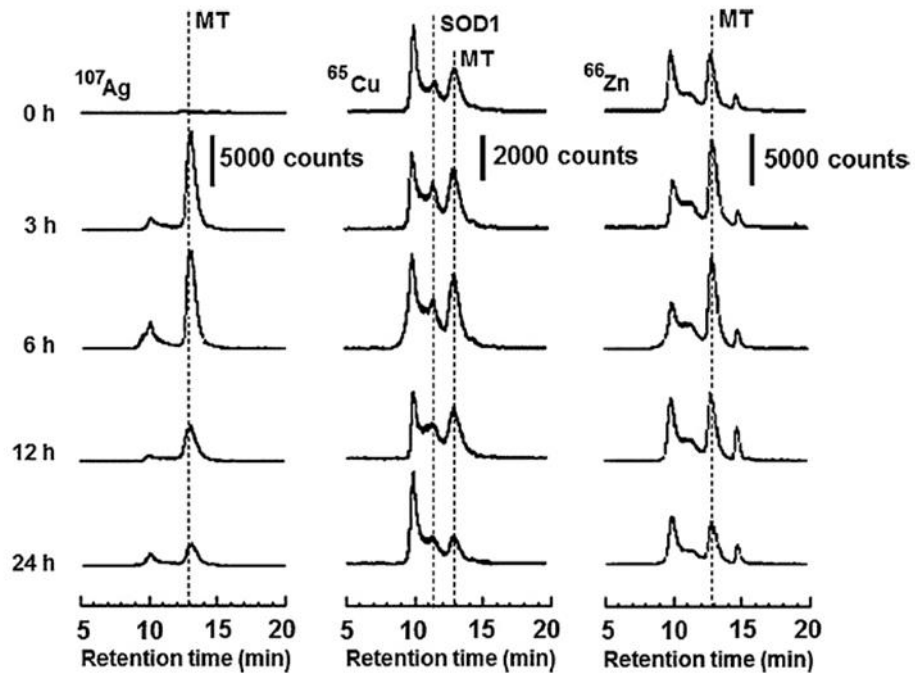


Fig.4

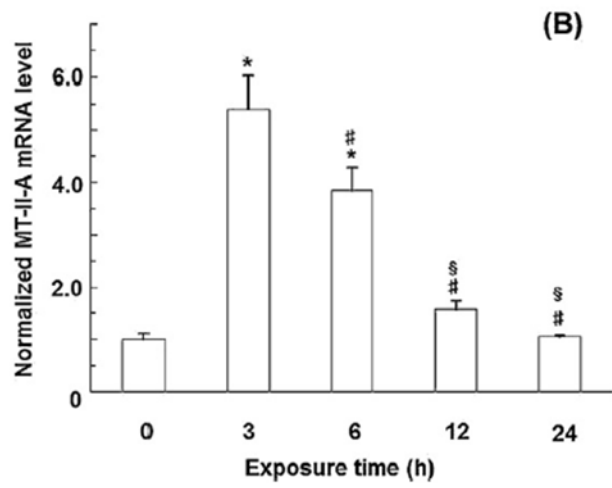
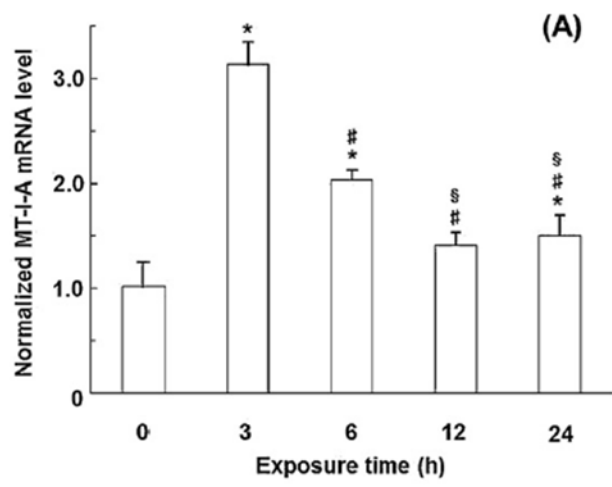


Fig.5

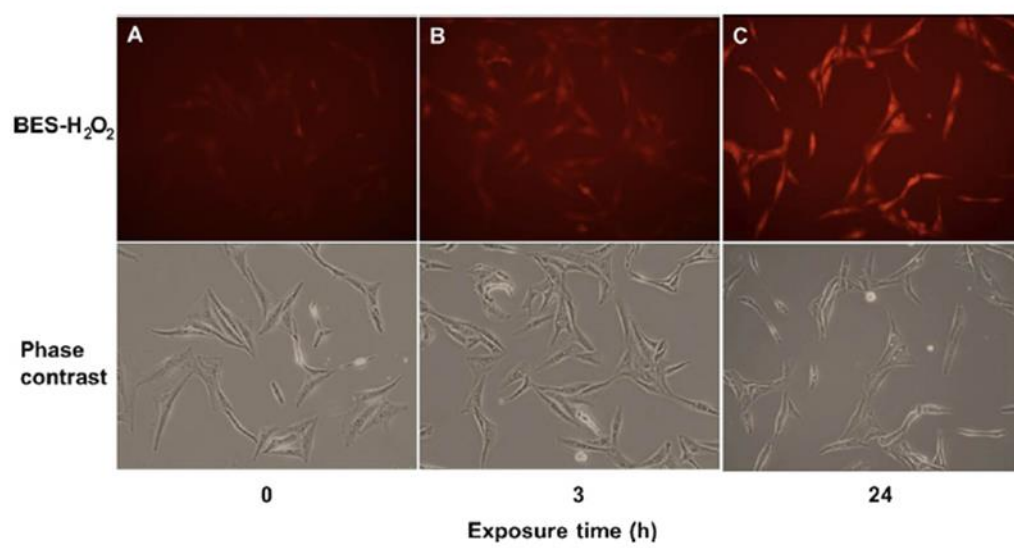


Fig.6

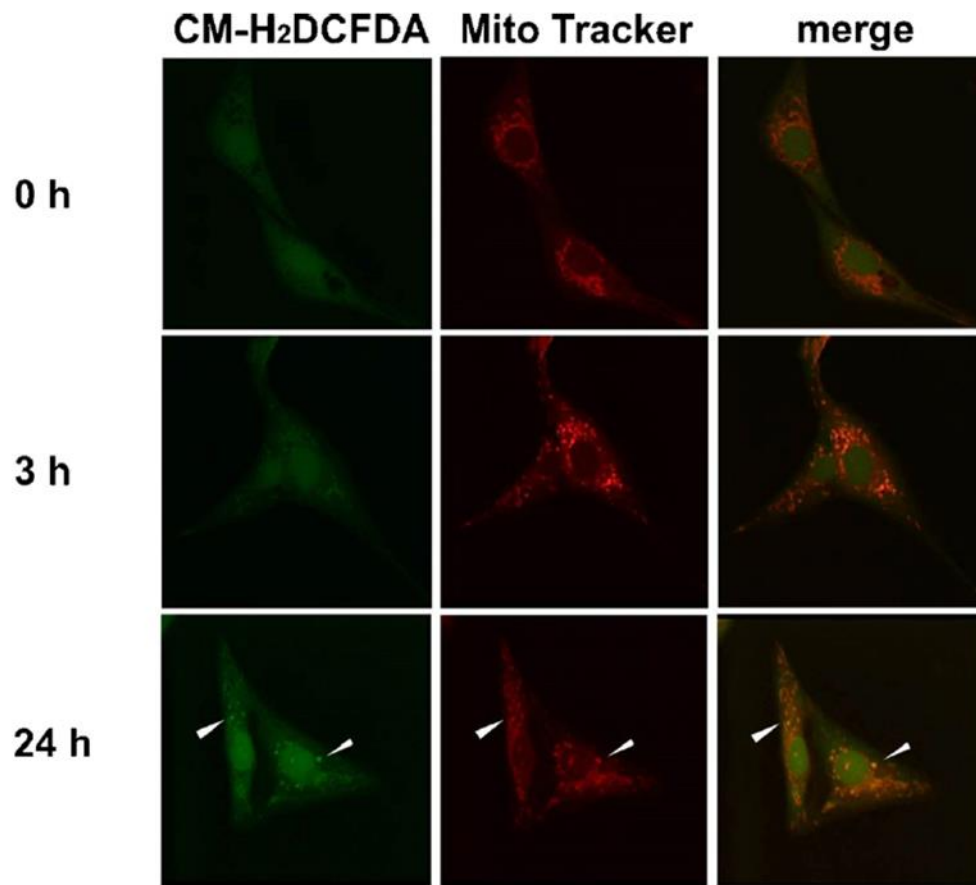


Fig.7

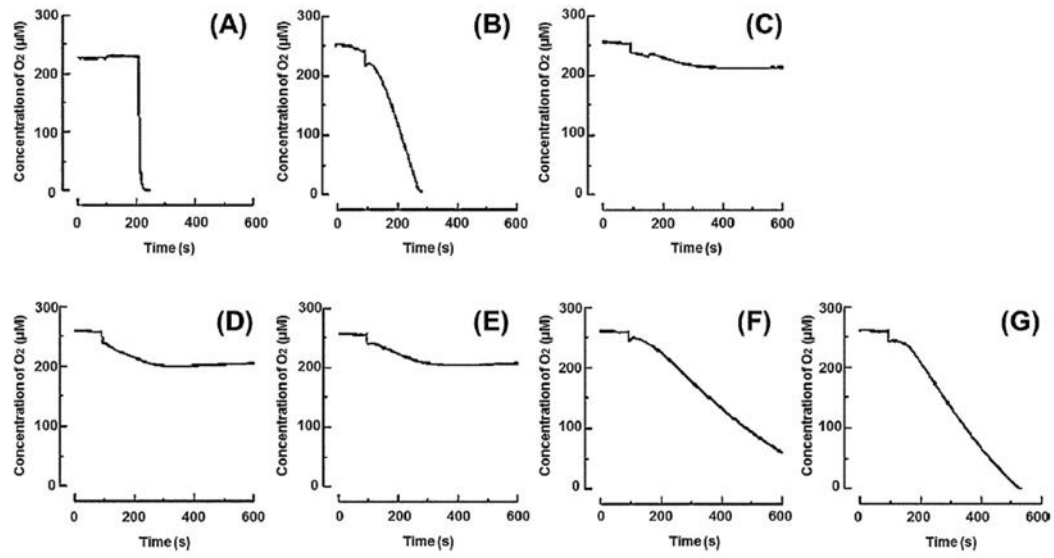


Fig.8

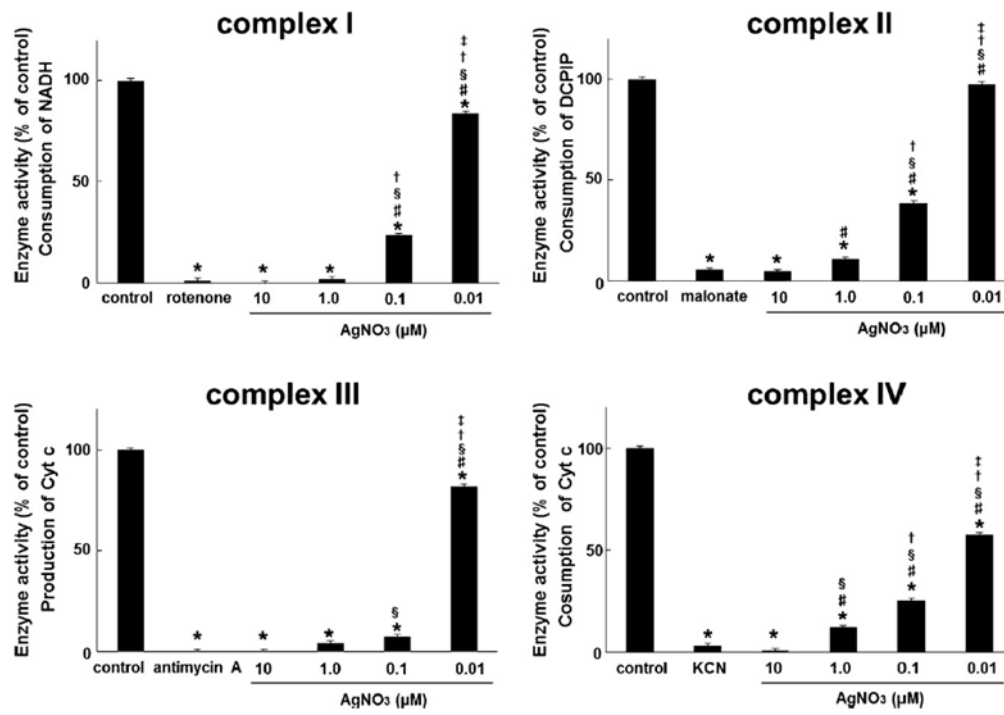


Fig.9

